ACS APPLIED MATERIALS & INTERFACES

www.acsami.org

Research Article

Insights into the Proton Transport Mechanism in TiO_2 Simple Oxides by *In Situ* Raman Spectroscopy

Jun Gao, Yuqing Meng, Allen Benton, Jian He, Luiz G. Jacobsohn, Jianhua Tong, and Kyle S. Brinkman*

Cite This: *ACS Appl. Mater. Interfaces* 2020, 12, 38012–38018

Read Online

ACCESS | Metrics & More | Article Recommendations | Supporting Information

ABSTRACT: Understanding the mechanisms of proton conduction at the interface of materials enables the development of a new generation of protonic ceramic conductors at low temperatures (<150 °C) through water absorption and proton transport on the surface and grain boundaries. Conductivity measurements under Ar-3% H_2O and Ar-3% D_2O revealed a $\sigma(H_2O)/\sigma(D_2O)$ ratio of approximately 2, indicating a hopping-based mechanism for proton conduction at the interface. *In situ* Raman spectroscopy was performed on water-saturated, porous, and nanostructured TiO_2 membranes to directly observe the isotope exchange reactions over the temperature range of 25 to 175 °C. The behavior of the isotope exchange reactions suggested a Grotthuss-type proton transport and faster isotope exchange reactions at 175 °C than that at 25 °C with a corresponding activation energy of 9 kJ mol^{-1}. The quantitative and mechanistic kinetic description of the isotope exchange process via *in situ* Raman spectroscopy represents a significant advance toward understanding proton transport mechanisms and aids in the development of high-performance proton conductors with rapid surface exchange coefficients of importance to contemporary energy conversion and storage material development. In addition, new material systems are proposed, which combine interface and bulk effects at low temperatures (<150 °C), resulting in enhanced proton transport through interfacial engineering at the nanoscale.

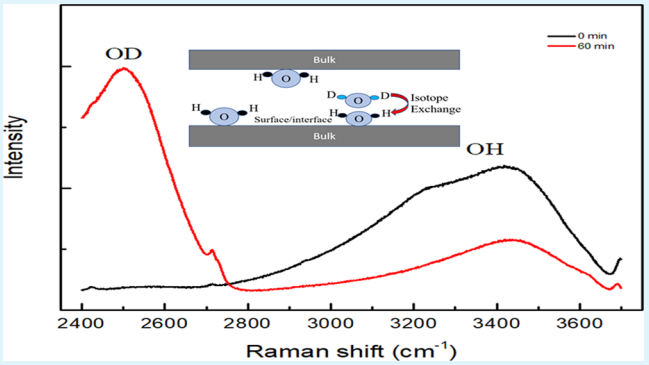

KEYWORDS: *proton transport, hydrogen isotope exchange, nanoscale TiO_2, protonic ceramic conductor, in situ Raman spectroscopy*

INTRODUCTION

Proton-conducting oxides have attracted interest due to their potential use in a wide range of electrochemical devices (protonic ceramic fuel cells,[1] electrolysers,[2] sensors,[3] and pumps[4]). The state-of-the-art high-temperature (>300 °C) protonic ceramic conductors are $BaZrO_3$- and $BaCeO_3$-based materials[2,5−7] in which protons can be incorporated into the bulk of the perovskite materials as protonic defects ($OH_{\ddot{O}}$) in the presence of hydrogen or water vapor-containing gases. The formation of protonic defects occurs through the following reactions:

$$H_2 + 2O_O^X \rightarrow 2OH_{\ddot{O}} + 2e' \quad (1)$$

$$H_2O + V_{\ddot{O}} + O_O^X \rightarrow 2OH_{\ddot{O}} \quad (2)$$

These materials exhibit high bulk proton conductivity over a wide temperature range (300 °C < T < 700 °C).[8] However, the total conductivity is limited by the blocking effect of the grain boundaries,[9] suggesting that an improved proton conductivity can be achieved by optimizing the characteristics of the interface. An alternative type of proton conductor, which relies on absorbed water at the surface and grain boundaries at low temperatures (<150 °C), has received increased attention.[10−13] Kim et al. showed the feasibility of power generation at low temperatures using water concentration cells with nanoscale fluorite-structured oxides as electrolytes.[14] Tredici et al. revealed that the proton conductivity strongly depends on the grain size, and the proton transport behavior cannot be explained by simple geometric brick-layer models, suggesting that the enhanced proton transport may rely on the space charge effects.[15] This phenomenon was also observed in other simple oxide systems, such as yttria-stabilized zirconia,[16,17] titanium oxide,[18] and ceria oxide.[19,20]

Proton conduction on nanocrystalline oxides primarily takes place in the chemisorbed and physisorbed water layers through hopping between water molecules according to the Grotthuss mechanism. In a recent review paper,[13] three temperature zones corresponding to different transport mechanisms of proton transport were defined in ionic conducting ceramic

Received: May 3, 2020
Accepted: July 28, 2020
Published: August 11, 2020

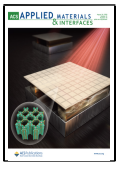

https://dx.doi.org/10.1021/acsami.0c08120
ACS Appl. Mater. Interfaces 2020, 12, 38012–38018

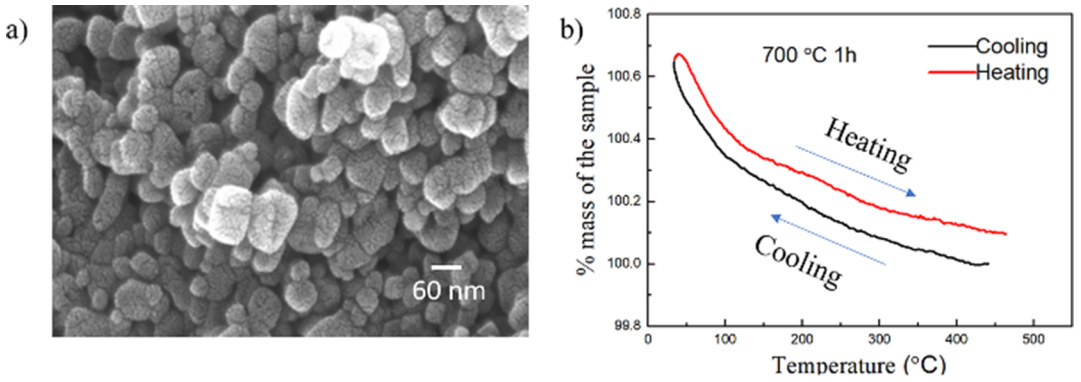

Figure 1. (a) Morphology of a TiO_2 porous membrane sintered at 700 °C for 1 h and (b) hydration and dehydration behaviors of the nanoscale TiO_2 membrane obtained from thermogravimetric analysis.

materials: zone 1 (T < 50 °C) occurs when physical absorption of water dominates; zone 2 (50 °C < T < 150 °C) occurs when a hydrogen bond network structure competes with physical adsorption water; and zone 3 (150 °C < T < 400 °C) occurs when chemical adsorption prevails. Interestingly, in zone 2, proton transport relies on the novel use of interfacial hydrated layers in ionic conducting ceramics by making use of the highly resistive interface presenting an opportunity for exploring a new generation of protonic ceramic conductors. A better understanding of the proton transport mechanism at the interface is crucial for material development. One way to directly evaluate the proton transport mechanism is by characterizing the H/D isotope exchange effect either by observing mass or conductivity change, such as thermogravimetric analysis and conductivity measurements,[21,22] or spectroscopic studies. Recently, Miyoshi et al. applied FT-IR to directly observe the isotope exchange reactions on nanostructured yttria-doped zirconia, observing faster isotope exchange rates at 400 °C than at 200 °C.[10] However, at present, there is a lack of kinetic description regarding the isotope exchange reactions on the interface of model oxide systems.

In this work, we present *in situ* Raman spectroscopy as a technique to directly identify the proton transport mechanism by quantifying the isotope exchange reactions on the oxides' interface. The behavior of the isotope exchange reactions suggested a Grotthuss-type proton transport and fast isotope exchange reactions at high temperatures with a corresponding activation energy of 9 kJ mol^{-1}. The results indicate that *in situ* Raman spectroscopy is an essential tool to aid understanding of proton transport mechanisms and assist in the development of a new generation of protonic ceramic conductors at low temperatures (<150 °C).

EXPERIMENTAL SECTION

Porous TiO_2 membranes were fabricated by a traditional ceramic sintering method. Nanoscale TiO_2 powders were pressed in a stainless die at 150 MPa and then sintered at 700 °C for 1 h in ambient air to form porous nanocrystalline pellets. Dense membranes were prepared by the spark plasma sintering (SPS) method. Powders were filled into a graphite die and sintered by SPS (Dr. Sinter 1020, Sumitomo Coal Mining Co.). This process was accomplished by applying a constant 5 kN axial force and an increasing current (100 A/min) simultaneously to the die in a dynamic vacuum (~10 Pa).

The morphology of TiO_2 membranes was evaluated by scanning electron microscopy (SEM, Hitachi S-4800). BET surface analyses were made using nitrogen physisorption (Quantachrome Autosorb iQ gas sorption analyzer). Thermogravimetric analysis (TGA 7, PerkinElmer) was used to analyze the water absorption and desorption processes in the nanostructured membranes. Initially, the temperature was increased to 450 °C with a heating rate of 1 °C/min to remove all molecular and absorbed water from the sample. Next, the temperature was decreased to room temperature under N_2-3% H_2O for the water absorption process. Finally, the sample was reheated back to 450 °C with the same heating rate used in the first step to observe the water desorption process from the membrane.

The conductivity of the TiO_2 membranes was tested by electrochemical impedance spectroscopy (EIS), using an electrochemical workstation (Solartron SI 1287 + 1260) at an alternating current (AC) amplitude of 100 mV in the frequency range from 1 to 100 MHz. Silver paste was printed onto both surfaces of the sintered membranes, working as the current collector. AC impedance plots were fitted using the ZView software according to the equivalent circuit.

Raman scattering spectra were recorded with a Horiba LabRAM HR Evolution Raman confocal microscope equipped with an 800 mm focal length spectrograph and a deep-depleted charge-coupled device detector using a 100 mW 532 nm laser with no attenuation, a 50× magnification objective, and 600 groves/mm diffraction gratings. The spectra corresponded to the accumulation of 10−15 s long scans. Each spectrum was corrected by the prerecorded instrument-specific response to a calibrated white light source, namely, the intensity correction system. Isotope exchange reactions were performed in a water-cooled hot stage (Linkam, TS1500) by changing the atmosphere from Ar-3% H_2O to Ar-3% D_2O at different temperatures (25 to 175 °C).

RESULTS AND DISCUSSION

Figure 1a displays the porous membranes with a relative density of 65.6% and a grain size of ~40 nm, and the diameter and thickness of the membrane are 0.6 and 0.19 cm, respectively. Figure 1 shows the water absorption and desorption processes observed by TGA measurements. During the cooling process from 450 °C to room temperature, water was absorbed to nearly 0.7 wt % of the sample. Most of the absorbed water was lost during the subsequent heating step to 450 °C. These results confirmed that the water absorption process occurred on the interface of nanostructured TiO_2 membranes below 450 °C.

The N_2 adsorption and desorption isotherms for the nanostructured TiO_2 membrane are reported in Figure 2. It is well known that a well-defined hysteresis loop is associated with the presence of open porosity producing capillary condensation of N_2. The surface area was 19.992 m^2/g, obtained by fitting the data with a BET isotherm, and the pore volume was found to be 7.675 × 10^{-2} cm^3/g, according to the total amount of the nitrogen absorbed at saturation.[23]

https://dx.doi.org/10.1021/acsami.0c08120
ACS Appl. Mater. Interfaces 2020, 12, 38012−38018

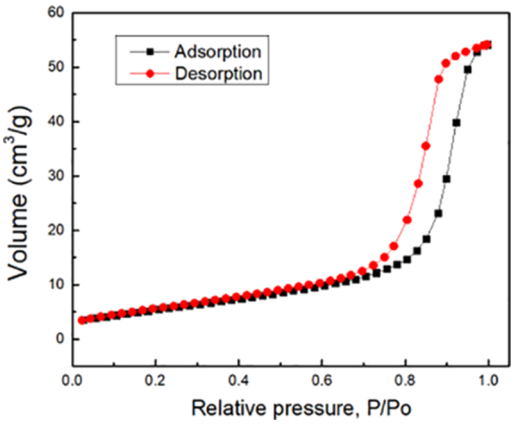

Figure 2. Nitrogen adsorption−desorption isotherms for nanostructured TiO_2 porous membranes.

Figure 3 shows the electrical conductivity of the as-prepared TiO_2 membrane exposed to different atmospheres and

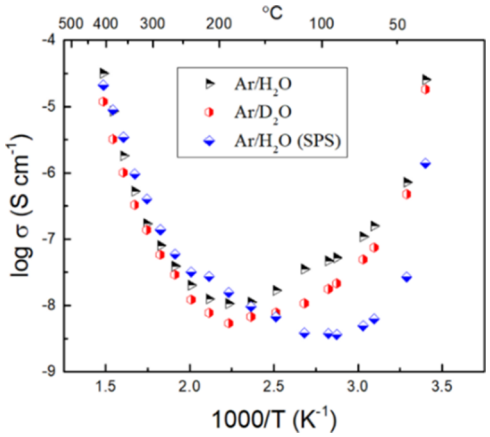

Figure 3. Total conductivity of a porous TiO_2 membrane under Ar-3% H_2O and Ar-3% D_2O and dense TiO_2 membrane fabricated by the SPS method under Ar-3% H_2O.

temperatures. The representative EIS plot of the nanostructure TiO_2 membrane under Ar-3% H_2O at 50 °C is given in Figure S1. The conductivity generally increased with increasing temperature above 150 °C, where proton transport occurred predominantly in the chemisorbed water layer.[16] With decreasing temperature, the activation energy gradually decreased, and the conductivity showed a thermally deactivated feature below 150 °C. The total conductivity increased with the decreasing temperature due to proton transport in the hydrogen-bonded and physically absorbed water layers. All observations agree with previous reports of proton conduction in porous ceramics.[10,11,14,16,18] A clear isotopic effect occurred when the mixture of Ar-3% D_2O was used. The conductivity in Ar-3% H_2O was clearly higher than that in Ar-3% D_2O, with a $(\sigma(H_2O)/\sigma(D_2O))$ ratio approximately around 2, close to the theoretical value of 1.4, suggesting hopping-based proton conduction on the oxides' interface.

For comparison, the total conductivity in dense membranes prepared by the SPS method is also included in Figure 3. The morphology (~40 nm) of the dense membrane is shown in Figure 4. The dense TiO_2 membrane showed a lower water absorption capacity (0.3 wt %) than the porous samples, as

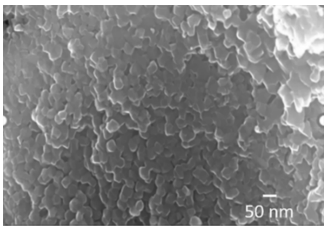

Figure 4. SEM image of a nanostructured TiO_2 membrane prepared by the SPS method at 700 °C for 5 min.

illustrated in Figure S2. As expected, the conductivity was lower in the dense membrane than in the porous membrane, resulting from the lower quantity of water absorption in dense membranes. In addition, the change between zones as defined by temperature-dependent conductivity measurements was lower in dense membranes than in porous membranes due to differences in the amount of water absorption.

In situ Raman spectroscopy was executed to confirm the OH and OD vibrations on the oxides' interface. The first chemisorbed layer above the oxides' interface consists of terminated and multicoordinated hydroxyls, followed by additional adsorption of the hydrogen-bonded water molecule, and then by physically absorbed water layers.[10,16] Representative Raman spectroscopy results of OH and OD vibrations measured from 25 to 300 °C are shown in Figure 5. The OH vibration appeared at ~3400 cm^{-1} with a shoulder at 3200 cm^{-1}, and the OD vibrations appeared at ~2550 cm^{-1}. Also, with increasing temperature, (1) the intensity of OH and OD vibrations decreased due to the reduced water absorption; (2) the main peaks shifted to higher wavenumbers due to different

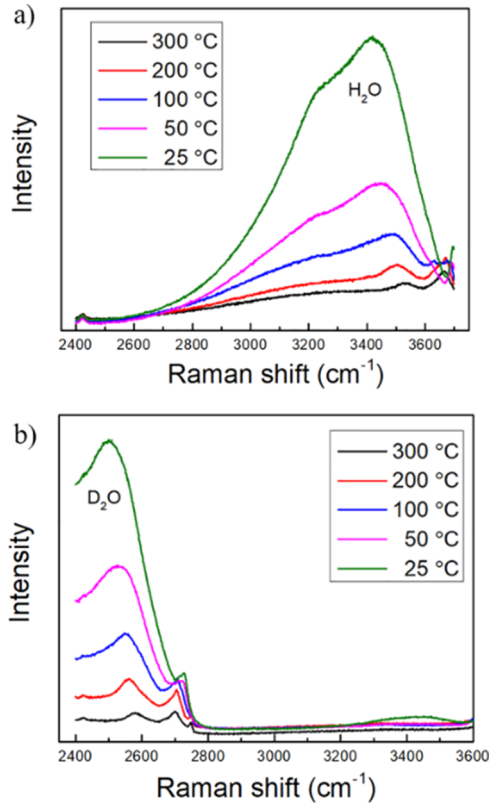

Figure 5. Representative (a) OH and (b) OD Raman vibrations from 25 to 300 °C under Ar-3% H_2O and Ar-3% D_2O, respectively.

https://dx.doi.org/10.1021/acsami.0c08120
ACS Appl. Mater. Interfaces 2020, 12, 38012−38018

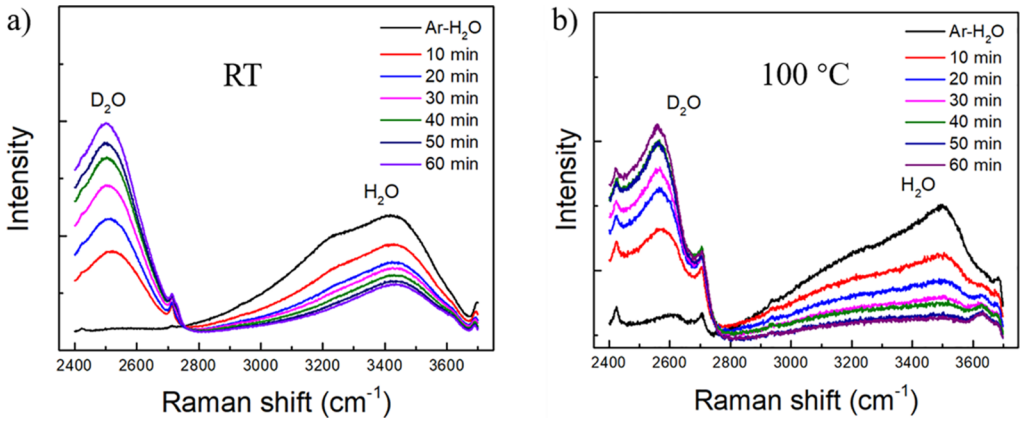

Figure 6. Temporal evolution of the Raman spectra of the TiO_2 membrane after switching the atmosphere from Ar-3% H_2O to Ar-3% D_2O at (a) room temperature (RT) and (b) 100 °C.

hydrogen bonding interactions (the stronger the hydrogen bond, the higher the shift in OH/OD stretching frequency); and (3) the width of the peaks were largely reduced in agreement with the previously reported spectra of OH and OD stretch band profiles.[24]

The exchange reactions of H_2O and D_2O were also studied by *in situ* Raman spectroscopy in order to provide insights into the proton transport mechanism. Spectra time evolution is shown in Figure 6, where the representative spectra in the range of 2400−3700 cm^{-1} are presented. These spectra were obtained after switching the atmosphere from Ar-3% H_2O to Ar-3% D_2O at room temperature and at 100 °C. The O−H vibration was immediately attenuated after the addition of D_2O to the atmosphere, as illustrated by changes to the ν_{OH} broad band at ∼3400 cm^{-1} and the ν_{OD} broad band at ∼2550 cm^{-1} due to the isotope exchange reactions of hydroxyl groups on the oxides' interface. The O−H vibration almost disappears after 30 min at 100 °C, indicating a faster isotope exchange rate at 100 °C than that observed at room temperature.

During the OH/OD exchange, the relevant variable was the fraction of remaining OH existing on the surface and grain boundaries of the nanostructured membrane, which was experimentally determined in terms of ratio $I_{OH}/I_{OH\ initial}$. As shown in Figure 7a, the decrease in the ν_{OH} integrated intensity follows a straight line in the semilogarithmic plot. It is therefore possible to define the first-order rate constant, $k_{H/D}$, as described in Amado and Ribeiro-Claro and Da Silvia et al.'s report.[25,26] Temperature-dependent measurements indicate that the exchange rates were appreciably faster at elevated temperatures. In a plot of $\ln(k)$ versus $1/T$, linear correlations were obtained for the isotope exchange reactions from Ar-3% H_2O to Ar-3% D_2O, suggesting an Arrhenius-type dependence of the rate constant. The resulting activation energy, E_a, of 9 kJ mol^{-1} was determined for the H/D exchange on the nanoscale oxides' surface and grain boundaries.

Table 1 displays a summary of H/D isotope exchange coefficient (k) and activation energy (E_a) in different material systems. The activation energy E_a for the H/D exchange found in this work, which is lower than the reported activation energy of 26 kJ mol^{-1} for the H/D exchange in β-cyclodextrin dodecahydrate, indicates that H/D exchange reactions occur more easily on the absorbed water of the oxides' surface than on the hydroxyl group in β-cyclodextrin dodecahydrate. The activation energy is comparable with that of the noble metal system for the D_2/H_2 exchange reactions. Interestingly, the

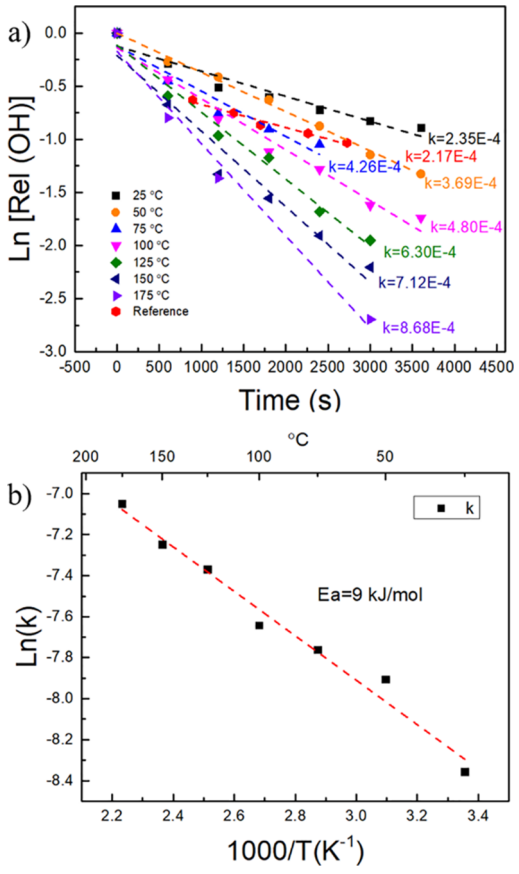

Figure 7. (a) Natural logarithm of the integrated relative Raman ν_{OH} intensity in a porous nanostructured TiO_2 membrane as a function of time of exposure to an atmosphere of Ar-3% D_2O together with the isotope exchange rate in β-cyclodextrin dodecahydrate[26] and (b) $\ln(k)$ vs $1/T$ for H/D isotope exchange reactions on the oxides' surface.

surface exchange coefficient (k) in nanoscale simple oxides is 100 times higher than that in the traditional oxidic protonic ceramic conductor ($SrCe_{0.95}Yb_{0.05}O_3$).[27] It is noted that this material was prepared by the solid state reaction method with a large grain size resulting in negligible water absorption on the surface and grain boundaries. This indicates that proton mobility at the interface in nanoscale simple oxide systems is much higher than the "bulk effect" of traditional protonic

https://dx.doi.org/10.1021/acsami.0c08120
ACS Appl. Mater. Interfaces 2020, 12, 38012−38018

Table 1. Summary of H/D Isotope Exchange Coefficient (k) at Room Temperature and Activation Energy (E_a) in Different Systems

exchange	materials	surface exchange rate (k, s^{-1})	activation energy (E_a, kJ mol^{-1})	method	reference
D_2O/H_2O	TiO_2	2.35×10^{-4}	9	*in situ* Raman	this work
D_2O/H_2O	$SrCe_{0.95}Yb_{0.05}O_3$	1.4×10^{-6}		elastic recoil detection	27
D_2O/H_2O	β-cyclodextrin dodecahydrate	2.17×10^{-4}	26	*in situ* Raman	26
D_2/H_2	β-phase palladium		3.5, 25	residual gas analyzer	28, 29

ceramic conductors at room temperature, which is consistent with the reported phenomenon in the nanoscale cerium oxide system.[30] From the TGA data, it is known that nanoscale TiO_2 membranes can absorb 0.03 mol water per mol TiO_2. If it is assumed that (i) the water layer in the nanostructured TiO_2 interface consists of a layer of physiosorbed water and a layer of chemisorbed water at room temperature,[16] (ii) the entire water content is absorbed on the surface and grain boundaries, and (iii) the monolayer water layer thickness is 0.282 nm,[31,32] according to the BET data, the surface and grain boundaries can accommodate $\sim 10^{22}$ protons cm^{-3} at room temperature. Therefore, the estimated interface concentration of protons is comparable to the calculated bulk content of protons derived from typical dopant concentrations (i.e., 15 mol % yttrium-doped $BaZrO_3$ has a proton concentration of $\sim 10^{21}$ protons cm^{-3}) of typical high-temperature protonic ceramic conductors found in the literature.[30]

Clearly, water absorption on the surface and grain boundaries in simple oxide systems has higher proton mobility and similar proton concentration as compared to the traditional high-temperature protonic ceramic conductors. Notably, the conductivity (σ, S/cm) follows eq 3, of which n is the carrier density (number of carriers/cm^3), q is the electric charge (C), and μ is the mobility (cm^2/Vs), qualitatively suggesting approximately 3 orders of magnitude higher interfacial conductivity as compared to the proton transport in high-temperature protonic ceramic conductors through bulk transport.[8,30]

$$\sigma = nq\mu \tag{3}$$

Figure 8 shows the water structure on the nanoscale oxides' interface[33] and proton defects[34] in the perovskite structure under a humidified atmosphere. These results indicate that when the grain size of protonic ceramic conductors is decreased, this will provide more active sites on the interface for water absorption, resulting in improved proton transport properties by combining the known "bulk effect" (proton defects) and newly discovered "interface effect" (absorbed water) in zone 2 (50 °C < T < 150 °C). This combination effect results in a conductive interface, which enhances ionic transport instead of blocking transport and provides a new promising solution for the development of a new generation of protonic ceramic conductors at low temperatures.

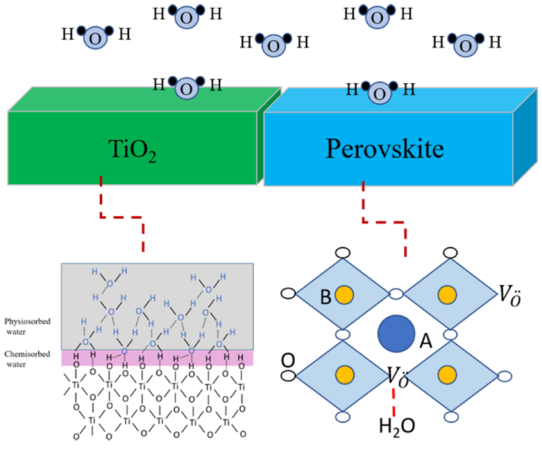

Figure 8. Illustration of the water structure on the nanoscale simple oxides' interface and proton defects forming in the perovskite structure under a humidified atmosphere.

CONCLUSIONS

In summary, *in situ* Raman spectroscopy was used to directly identify the proton transport mechanism on the interface of nanostructured ceramic membranes. The observed isotope exchange reactions on the interface indicate a Grotthuss- or "hopping"-type mechanism of proton transport, which is selective to isotopes due to mass differences. Fast isotope exchange reactions with an activation energy of 9 kJ mol^{-1} for the H/D exchange on the oxides' surface were observed in simple oxides, which was over 100 times higher than that of the traditional oxidic proton conductors. In addition, the estimated surface concentration of protons in simple oxides is comparable to the calculated bulk content of protons for typical perovskite-based proton conductors, indicating the potential for enhanced proton conduction. Based on these results, new material systems were proposed, which combine interface and bulk effects in an intermediate temperate range, resulting in a promising new solution for the development of advanced ionic conductors through interfacial engineering at the nanoscale.

ASSOCIATED CONTENT

Supporting Information

The Supporting Information is available free of charge at https://pubs.acs.org/doi/10.1021/acsami.0c08120.

Representative EIS plot for the porous TiO_2 membrane at 50 °C; water absorption from TGA of the TiO_2 dense membrane; and XRD patterns for porous and dense membranes (PDF)

AUTHOR INFORMATION

Corresponding Author

Kyle S. Brinkman − *Department of Materials Science and Engineering and Center for Nuclear Environment Engineering Sciences and Radioactive Waste Management (NEESRWM), Clemson University, Clemson, South Carolina 29634, United States;* orcid.org/0000-0002-2219-1253; Email: ksbrink@clemson.edu

Authors

Jun Gao − *Department of Materials Science and Engineering, Clemson University, Clemson, South Carolina 29634, United States*

https://dx.doi.org/10.1021/acsami.0c08120
ACS Appl. Mater. Interfaces 2020, 12, 38012−38018

Yuqing Meng − *Department of Materials Science and Engineering, Clemson University, Clemson, South Carolina 29634, United States*

Allen Benton − *Department of Physics and Astronomy, Clemson University, Clemson, South Carolina 29634, United States*

Jian He − *Department of Physics and Astronomy, Clemson University, Clemson, South Carolina 29634, United States;* orcid.org/0000-0002-6377-3022

Luiz G. Jacobsohn − *Department of Materials Science and Engineering and Center for Nuclear Environment Engineering Sciences and Radioactive Waste Management (NEESRWM), Clemson University, Clemson, South Carolina 29634, United States*

Jianhua Tong − *Department of Materials Science and Engineering and Center for Nuclear Environment Engineering Sciences and Radioactive Waste Management (NEESRWM), Clemson University, Clemson, South Carolina 29634, United States;* orcid.org/0000-0002-0684-1658

Complete contact information is available at: https://pubs.acs.org/10.1021/acsami.0c08120

Author Contributions

The manuscript was written with contributions of all authors. All authors have given approval to the final version of the manuscript.

Funding

The research is funded by DOE-NEUP/CFA-17-12,798.

Notes

The authors declare no competing financial interest.

■ ACKNOWLEDGMENTS

The authors gratefully acknowledge the award DE-NE0008703 from the Department of Energy, Nuclear Energy Research Programs (DOE-NEUP) for project CFA-17-12798: Nanostructured Ceramic Membranes for Enhanced Tritium Management.

■ REFERENCES

(1) Duan, C.; Tong, J.; Shang, M.; Nikodemski, S.; Sanders, M.; Ricote, S.; Almansoori, A.; O'Hayre, R. Readily Processed Protonic Ceramic Fuel Cells with High Performance at Low Temperatures. *Science* **2015**, *349*, 1321−1326.

(2) Duan, C.; Kee, R. J.; Zhu, H.; Karakaya, C.; Chen, Y.; Ricote, S.; Jarry, A.; Crumlin, E. J.; Hook, D.; Braun, R.; Sullivan, N. P.; O'Hayre, R. Highly Durable, Coking and Sulfur Tolerant, Fuel-Flexible Protonic Ceramic Fuel Cells. *Nature* **2018**, *557*, 217−222.

(3) Hübert, T.; Boon-Brett, L.; Black, G.; Banach, U. Hydrogen Sensors − A Review. *Sens. Actuators, B* **2011**, *157*, 329−352.

(4) Iwahara, H. Hydrogen Pumps Using Proton-Conducting Ceramics and Their Applications. *Solid State Ionics* **1999**, *125*, 271−278.

(5) Fabbri, E.; D'Epifanio, A.; Di Bartolomeo, E.; Licoccia, S.; Traversa, E. Tailoring the Chemical Stability of Ba $(Ce_{0.8-x}Zr_x)Y_{0.2}O_{3-\delta}$ Protonic Conductors for Intermediate Temperature Solid Oxide Fuel Cells (IT-SOFCs). *Solid State Ionics* **2008**, *179*, 558−564.

(6) Yang, L.; Wang, S.; Blinn, K.; Liu, M.; Liu, Z.; Cheng, Z.; Liu, M. Enhanced Sulfur and Coking Tolerance of a Mixed Ion Conductor for SOFCs: $BaZr_{0.1}Ce_{0.7}Y_{0.2-X}Yb_xO_{3-\delta}$. *Science* **2009**, *326*, 126−129.

(7) Gao, J.; Meng, Y.; Hong, T.; Kim, S.; Lee, S.; He, K.; Brinkman, K. S. Rational Anode Design for Protonic Ceramic Fuel Cells by a One-Step Phase Inversion Method. *J. Power Sources* **2019**, *418*, 162−166.

(8) Kreuer, K. D. Proton-Conducting Oxides. *Annu. Rev. Mater. Res.* **2003**, *33*, 333−359.

(9) Shirpour, M.; Merkle, R.; Maier, J. Space Charge Depletion in Grain Boundaries of $BaZrO_3$ Proton Conductors. *Solid State Ionics* **2012**, *225*, 304−307.

(10) Miyoshi, S.; Akao, Y.; Kuwata, N.; Kawamura, J.; Oyama, Y.; Yagi, T.; Yamaguchi, S. Low-Temperature Protonic Conduction Based on Surface Protonics: An Example of Nanostructured Yttria-Doped Zirconia. *Chem. Mater.* **2014**, *26*, 5194−5200.

(11) Scherrer, B.; Schlupp, M. V. F.; Stender, D.; Martynczuk, J.; Grolig, J. G.; Ma, H.; Kocher, P.; Lippert, T.; Prestat, M.; Gauckler, L. J. On Proton Conductivity in Porous and Dense Yttria Stabilized Zirconia at Low Temperature. *Adv. Funct. Mater.* **2013**, *23*, 1957−1964.

(12) Park, H. J.; Roh, J. W. Protonic Conduction of Nanostructured Y-Doped $BaZrO_3$. *J. Nanomater.* **2016**, *2016*, 1−6.

(13) Meng, Y.; Gao, J.; Zhao, Z.; Amoroso, J.; Tong, J.; Brinkman, K. S. Review: Recent Progress in Low-Temperature Proton-Conducting Ceramics. *J. Mater. Sci.* **2019**, *54*, 9291−9312.

(14) Kim, S.; Anselmi-Tamburini, U.; Park, H. J.; Martin, M.; Munir, Z. A. Unprecedented Room-Temperature Electrical Power Generation Using Nanoscale Fluorite-Structured Oxide Electrolytes. *Adv. Mater.* **2008**, *20*, 556−559.

(15) Tredici, I. G.; Maglia, F.; Ferrara, C.; Mustarelli, P.; Anselmi-Tamburini, U. Mechanism of Low-Temperature Protonic Conductivity in Bulk, High-Density, Nanometric Titanium Oxide. *Adv. Funct. Mater.* **2014**, *24*, 5137−5146.

(16) Stub, S. Ø.; Vøllestad, E.; Norby, T. Mechanisms of Protonic Surface Transport in Porous Oxides: Example of YSZ. *J. Phys. Chem. C* **2017**, *121*, 12817−12825.

(17) Köck, E.-M.; Kogler, M.; Klötzer, B.; Noisternig, M. F.; Penner, S. Structural and Electrochemical Properties of Physisorbed and Chemisorbed Water Layers on the Ceramic Oxides Y_2O_3, YSZ, and ZrO_2. *ACS Appl. Mater. Interfaces* **2016**, *8*, 16428−16443.

(18) Maglia, F.; Tredici, I. G.; Spinolo, G.; Anselmi-Tamburini, U. Low Temperature Proton Conduction in Bulk Nanometric TiO_2 Prepared by High-Pressure Field Assisted Sintering. *J. Mater. Res.* **2012**, *27*, 1975−1981.

(19) Gregori, G.; Shirpour, M.; Maier, J. Proton Conduction in Dense and Porous Nanocrystalline Ceria Thin Films. *Adv. Funct. Mater.* **2013**, *23*, 5861−5867.

(20) Chueh, W. C.; Yang, C.-K.; Garland, C. M.; Lai, W.; Haile, S. M. Unusual Decrease in Conductivity upon Hydration in Acceptor Doped, Microcrystalline Ceria. *Phys. Chem. Chem. Phys.* **2011**, *13*, 6442.

(21) Hancke, R.; Li, Z.; Haugsrud, R. Thermogravimetric Relaxation Study of the Proton Conductor Lanthanum Tungstate, $La_{28-x}W_{4+x}O_{54+\delta}v_{2-\delta}$, x = 0.85. *Int. J. Hydrogen Energy* **2012**, *37*, 8043−8050.

(22) Slade, R. C. T.; Singh, N. Generation of Charge Carriers and an H/D Isotope Effect in Proton-Conducting Doped Barium Cerate Ceramics. *J. Mater. Chem.* **1991**, *1*, 441.

(23) Lowell, S.; Shields, J. E.; Thomas, M. A.; Thommes, M. *Characterization of Porous Solids and Powders: Surface Area, Pore Size and Density*; Springer: Dordrecht, 2012.

(24) Hu, Q.; Zhao, H.; Ouyang, S. Understanding Water Structure from Raman Spectra of Isotopic Substitution H_2O/D_2O up to 573 K. *Phys. Chem. Chem. Phys.* **2017**, *19*, 21540−21547.

(25) Amado, A. M.; Ribeiro-Claro, P. J. A. H/D and D/H Exchange Rates in α-Cyclodextrin and α-Cyclodextrin Inclusion Compounds Raman Spectroscopic study. *J. Chem. Soc., Faraday Trans.* **1997**, *93*, 2387−2390.

(26) Da Silva, A. M.; Steiner, T.; Saenger, W.; Empis, J.; Teixeira-Dias, J. J. C. Dynamics of H/D and D/H Exchanges in β-Cyclodextrin Dodecahydrate Observed in Real Time: Effects from Zero-Point Vibrational Energy. *Chem. Commun.* **1997**, *5*, 465−466.

(27) Iizuka, E.; Horikawa, T.; Tsuchiya, B.; Soda, K.; Morita, K.; Iwahara, H. Anomalous Difference between Replacements of D−H and H−D in Oxide Ceramics by Exposure to Air Containing H_2O and D_2O Vapors. *Jpn. J. Appl. Phys.* **2001**, *40*, 3343−3348.

(28) Luo, W.; Cowgill, D. F.; Causey, R. A. Thermodynamic and Kinetic Characterization of Hydrogen−Deuterium Exchange in β-Phase Palladium. *J. Phys. Chem. B.* **2009**, *113*, 12978−12987.
(29) Luo, W.; Cowgill, D. F. Kinetics of Hydrogen Isotope Exchange in β-Phase Pd−H−D. *J. Phys. Chem. C* **2015**, *119*, 18099−18109.
(30) Shirpour, M.; Gregori, G.; Merkle, R.; Maier, J. On the Proton Conductivity in Pure and Gadolinium Doped Nanocrystalline Cerium Oxide. *Phys. Chem. Chem. Phys.* **2011**, *13*, 937−940.
(31) Asay, D. B.; Kim, S. H. Evolution of the Adsorbed Water Layer Structure on Silicon Oxide at Room Temperature. *J. Phys. Chem. B.* **2005**, *109*, 16760−16763.
(32) Stub, S. Ø.; Vøllestad, E.; Norby, T. Protonic Surface Conduction Controlled by Space Charge of Intersecting Grain Boundaries in Porous Ceramics. *J. Mater. Chem. A* **2018**, *6*, 8265−8270.
(33) Wu, C.-Y.; Tu, K.-J.; Deng, J.-P.; Lo, Y.-S.; Wu, C.-H. Markedly Enhanced Surface Hydroxyl Groups of TiO_2 Nanoparticles with Superior Water-Dispersibility for Photocatalysis. *Materials* **2017**, *10*, 566.
(34) Zhou, Y.; Guan, X.; Zhou, H.; Ramadoss, K.; Adam, S.; Liu, H.; Lee, S.; Shi, J.; Tsuchiya, M.; Fong, D. D.; Ramanathan, S. Strongly Correlated Perovskite Fuel Cells. *Nature* **2016**, *534*, 231−234.

https://dx.doi.org/10.1021/acsami.0c08120
ACS Appl. Mater. Interfaces 2020, 12, 38012−38018